Sensors and Materials, Vol. 37, No. 3 (2025) 921–942
MYU Tokyo

S & M 3966

Addressing Time Variance in Measurement Systems with Bayesian Model Updating

Jan-Hauke Bartels* and Steffen Marx

Institute of Concrete Structures, TUD Dresden University of Technology,
Helmholtzstr. 10, 01069 Dresden, Germany

(Received November 6, 2024; accepted January 28, 2025)

Keywords: Bayesian model updating, laser triangulation sensor, sensor aging, time-variant system behavior, uncertainty quantification

Measurement systems are widely used in engineering applications such as structural health monitoring and nondestructive evaluation to enhance periodic inspections with continuous data acquisition. These systems are often assumed to exhibit linear time-invariant behavior, although over time, their performance is affected by environmental factors and internal degradation, resulting in time-variant behavior. In this study, we investigated the effects of aging on measurement systems, using laser triangulation sensors as a case study, and propose a novel approach to compensate for these time-dependent effects. Through a series of more than 140 subtests, we identified both random and systematic measurement errors, such as those caused by cable length, sensor placement, and temperature variations. We introduced a compensation method based on Bayesian model updating (BMU) that effectively accounts for the time-dependent drift in measurement accuracy, especially in the early stages of sensor aging. The BMU model was validated through experiments, demonstrating its ability to mitigate aging-induced measurement errors with high accuracy. In this work, we highlight the importance of compensating for time-variant behavior and provide a reliable approach to ensuring measurement accuracy in long-term measurement systems. The results are applicable to various engineering applications and contribute to improving the longevity and reliability of monitoring systems.

1. Motivation and Objective

Today, measurement systems are used in many fields of application. In engineering, structural health monitoring (SHM) and nondestructive evaluation are increasingly used in practice to improve periodic inspections of engineering structures with continuous measurement data.[1–3]

Since measurement systems have high precision, linear time-invariant (LTI) system behavior is often assumed. An LTI system adheres to the principles of linearity (additivity and homogeneity) and time invariance.

*Corresponding author: e-mail: jan-hauke.bartels@tu-dresden.de
https://doi.org/10.18494/SAM5393

ISSN 0914-4935
https://myukk.org/

$$\text{Linearity:} \quad \begin{aligned} &\text{If } x_1(t) \to y_1(t) \text{ and } x_2(t) \to y_2(t), \text{ then } x_1(t) + x_2(t) \to y_1(t) + y_2(t), \text{ and} \\ &\text{If } x(t) \to y(t), \text{ then } a \cdot x(t) \to a \cdot y(t) \end{aligned} \tag{1}$$

$$\text{Time invariance:} \quad \text{If } x(t) \to y(t), \text{then } x(t - t_0) \to y(t - t_0) \tag{2}$$

Here, $x(\cdot)$ is the input signal and $y(\cdot)$ is the output signal over time t. Since engineering structures are designed for a service life of several decades (e.g., wind turbines for 25 years, bridges for 100 years), changes occur in the structure, such as deterioration-related damage, and under environmental conditions such as climate change or changing operational management throughout its life cycle. Monitoring systems must reliably detect these changes. However, the problem is that, on the one hand, the structure degrades over its lifetime, and, on the other hand, the monitoring system itself is subject to an aging process and becomes less reliable.[4–6] The assumption of time invariance is no longer valid. This time-variant behavior of the measurement system must be identified and compensated for in the monitoring process.

The processing of monitoring data generally involves four steps,[7] as illustrated in Fig. 1.

The operational evaluation defines the components and changes in condition to be monitored and selects the appropriate measurement principles and sensors. These sensors are installed and calibrated on the object to be measured. They continuously measure the behavior of the components and transmit the data in a time-synchronized manner to a database. During data processing, the raw data is filtered, cleaned, and normalized. The monitoring characteristics are then analyzed to evaluate the condition of the structure and to detect changes in condition. This process allows the early detection of changes in condition, resulting in less frequent inspections on site and savings in manpower and costs.[8] Data normalization in particular is crucial for the quality of measurement evaluation. Effects such as a change in temperature have been shown to have a significant impact on measurements.[9] Without compensation for these effects, incorrect conclusions can be drawn about the condition of the measurement object.

In this regard, the distinction between structural damage and sensor failure is a critical point, as the components of the measurement system do not fail immediately but gradually deteriorate, incorporating time-variant behavior. To solve this problem, the basic method of sensor fault diagnosis can be used. According to Patton, sensor fault diagnosis includes (i) fault detection, (ii) fault location, (iii) fault classification, and (iv) fault compensation.[10] The concept of fault diagnosis has been intensively studied in computer science for several years.[11–14] We also

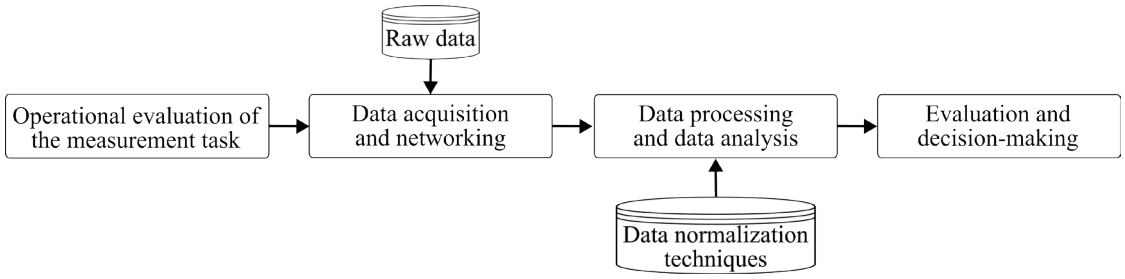

Fig. 1. Workflow to handle monitoring data.

described a possible method for detecting and localizing sensor faults in another paper.[15] However, what is missing in these papers is the compensation for such time-variant effects. Thus, in this paper, we focus on the compensation of aging effects in measurement systems as part of the process of handling monitoring data in the data normalization step. With laser triangulation as a case study, this research is applicable to other measurement principles. The following questions are addressed: (i) What random and systematic effects on measurement systems must be considered in engineering applications to define an analytical model for measurement system behavior? (ii) How can time-dependent changes in the measurement system be compensated for?

This paper is organized as follows: In Sect. 2, we describe the methodology for the monitoring of aging monitoring systems and show the experimental setup and the test procedure used. In Sect. 3, we present the analysis and evaluation of the time-invariant and time-variant measurement system behaviors. In Sect. 4, we provide an approach to address the behavior of a time-variant system using Bayesian model updating (BMU). In Sect. 5, we conclude with a summary and outlook. This work demonstrates an innovative approach to compensate for aging measurement systems that will make monitoring systems even more reliable for long-lasting engineering structures.

2. Methodology and Experimental Setup

2.1 Method for handling time-variant monitoring systems

In principle, the measurement signal for handling time-variant monitoring systems can be described additively by random and systematic measurement errors, where systematic measurement errors are divided into temperature-dependent and time-dependent systematic errors:

$$y = y_{True} + \epsilon_{Temperature} + \epsilon_{Aging} + \epsilon_{Random}, \tag{3}$$

where y_{True} is the true value of the measured variable, $\epsilon_{Temperature}$ represents the temperature-dependent systematic error of a measurement, ϵ_{Aging} accounts for the time-dependent systematic error of a measurement, and ϵ_{Random} describes the random error of a measurement.

As systematic measurement errors originate from different sources, they are explicitly separated into temperature and aging effects. This distinction enables a more precise correction approach, as both effects may change over time with different characteristics. Consequently, the mathematical model of the measurement system must account for these two sources from the very beginning.

In practice, the true value y_{True} is approximated by the mean $\bar{y}$ of the measurements, while the random errors are often described by the twofold standard deviation σ. The systematic error must be determined and corrected separately if it is known. This correction corresponds to the data normalization technique described in Fig. 1. Therefore, the analytical description of the behavior of a measurement system can be given by

$$y = \bar{y} + \epsilon_{Temperature} + \epsilon_{Aging} \pm 2 \cdot \sigma \cdot \tag{4}$$

With this knowledge, the workflow for describing and handling the time-dependent behavior of measurement systems can be shown in Fig. 2.

The process begins with the raw data recorded. The first task is to model the measurement by describing the effects on the measurement system. A distinction is made between random and systematic effects so that the mathematical model can be set up according to Eq. (3). The second task is to deal with the aging of the measurement system. It can be assumed that the mathematical model also changes, so it must be adjusted. This adjustment must be done using a probabilistic approach since the mathematical model contains not only the mean but also the measurement uncertainty. BMU is suitable for this purpose. Compared with machine learning (ML) regression models such as neural networks or Gaussian processes, BMU offers several key advantages:

- Uncertainty quantification: BMU directly incorporates uncertainty via probability distributions, ensuring transparent and robust estimates of parameters and predictions.
- Leverage prior knowledge: BMU uses prior distributions, enabling accurate fits even with limited or noisy data, unlike ML models, which depend on large datasets.
- Flexibility and interpretability: BMU adapts to different models and data structures, offering clear insights into parameter uncertainties. In contrast, complex ML models often act as "black boxes", limiting their interpretability.

The principle of BMU is introduced briefly here, with further details available in the literature.[16,17] In engineering, computational models are used to simulate physical systems under different conditions. However, owing to incomplete information, discrepancies often arise between theoretical predictions and real-world observations. BMU helps bridge this gap by reducing the errors between model predictions and actual data. Measured data refine these input parameters to improve the accuracy of the computational model. BMU is applied in various engineering fields, such as tracking stiffness degradation in wind turbines,[18] predicting fatigue crack growth in steel pipes,[19] and identifying cracks in building structures via SHM.[20] We are not aware of any application to compensate for aging effects within the measurement systems themselves.

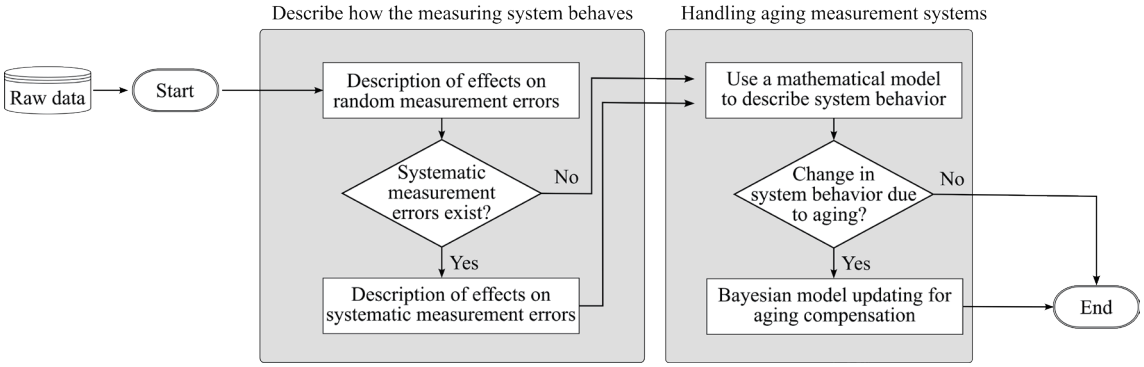

Fig. 2. Proposed method to handle aging of the measurement system.

Consider a set of uncertain input parameters $\boldsymbol{\Theta} = \{\Theta_1, \Theta_2, \ldots\}$ for a model $M(\boldsymbol{\Theta})$. Let $\boldsymbol{D} = \{D_i\}\_(i = 1, ..., N_{obs})$ represent N_{obs} recorded data, which can be computed using $M(\boldsymbol{\Theta})$. The uncertainty in $\boldsymbol{\Theta}$ is captured using a probability density function (PDF) $p(\boldsymbol{\Theta})$. Since the joint PDF is not initially known, BMU updates the prior distribution $p(\boldsymbol{\Theta})$ using the observed data $\boldsymbol{D}$, inferring the posterior distribution $p(\boldsymbol{\Theta} \mid \boldsymbol{D})$ via the Bayes theorem:

$$p(\theta \mid \boldsymbol{D}) = \frac{\mathcal{L}(\boldsymbol{D} \mid \theta) \cdot p(\theta)}{p(\boldsymbol{D})}. \tag{5}$$

Here, $p(\theta)$ is the prior distribution, based on expert knowledge or laboratory experiments. A common prior is an uninformative uniform prior, based on maximum entropy.[21] Bounds are selected to enclose the posterior distribution. The likelihood $\mathcal{L}(\boldsymbol{D} \mid \theta)$ describes the error between the observed data $\boldsymbol{D}$ and the model $M(\theta)$, typically assuming a Gaussian likelihood with zero mean and a fixed standard deviation. The denominator $p(\boldsymbol{D})$ ensures that the posterior integrates to one. Since the posterior geometry is unknown and may be multimodal, sampling from it is challenging. Therefore, different sampling methods have been developed to solve this problem. The most commonly used are the Markov Chain Monte Carlo (MCMC) sampler or the transitional Markov Chain Monte Carlo (TMCMC) sampler.[16] Both samplers were used in this study and their performance characteristics in the update of the measurement system behavior were compared.

2.2 Experimental setup for time-invariant and time-variant tests

In this section, we describe the measurement concept for the tested sensor type (laser triangulation sensor, LTS), including the measurement system components and signal processing. Figure 3 shows the experimental setup, showing six sensors analyzed for time-invariant and time-variant behaviors.

The climatic chamber has a test volume of 2.00 × 2.00 × 2.00 m^3 and is equipped with a frequency-controlled cooling unit for heat removal, an air cooler for uniform temperature distribution (down to –25 °C), and a tube heater for heating up to +100 °C. It also includes an ultrasonic humidifier and an adsorption dryer to control relative humidity from 25 to 85%. The chamber allows for programmable temperature and humidity cycles for periodic analysis.

The measurement system, which includes LTS, cable, and measurement module, is housed in a climatic chamber. The LTS, mounted on a base plate and upstand made of Alloy 36 (with a coefficient of thermal expansion $\alpha_{T,\,\mathrm{Alloy36}} = 0.50 \cdot 10^{-6}\,\mathrm{K}^{-1}$), measures the horizontal distance to the upstand. For comparison, structural steel has a thermal expansion coefficient more than 20 times higher ($\alpha_{T,\,\mathrm{Steel}} = 13.00 \cdot 10^{-6}\ \mathrm{K}^{-1}$), making the expansion of the base plate negligible. Table 1 shows the characteristics of the sensors used.

Current output LTSs have a measurement range of 0–10 mm and measure at distances between 16 and 26 mm, whereas voltage output LTSs have a measurement range of 0–500 mm and can measure between 50 and 550 mm. The repeatability (random measurement error) values

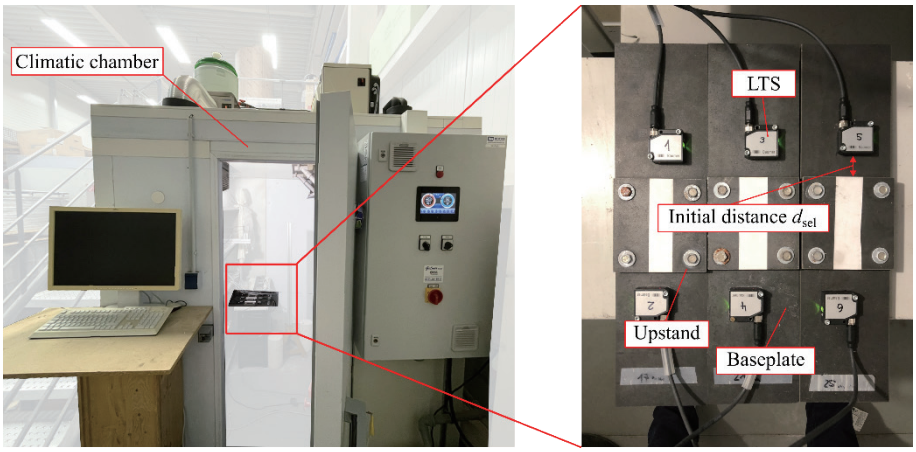

Fig. 3. (Color online) Experimental setup for time-invariant and time-variant LTS tests. (a) LTS test setup in the climatic chamber and (b) detailed view of the LTS test setup.

Table 1
Characteristics of the LTSs used.

Manufacturer	Baumer Holding AG, Switzerland	Baumer Holding AG, Switzerland
Model name	OM20-P0026.HH.YIN	OM30-L0550.HV.YUN
Output	Electrical current	Electrical voltage
Number of sensors tested	6	3
Measurement distance (Sd)	16–26 mm	50–550 mm
Measurement range (MR)	0–10 mm	0–500 mm
Repeatability (random measurement error)	±1 µm (= $1 \cdot 10^{-6}$ mm)	±2–86 µm (= $2 \cdot 10^{-6}$–$86 \cdot 10^{-6}$ mm)
Output signal	4–20 mA (Current output)	0–10 V (Voltage output)
Temperature dependence	0.01% Sde/K	0.08% Sde/K

of these sensors are ±1 µm and ±2–86 µm, respectively.[22] The sensors used in our study are temperature-dependent. The unit Sde/K is defined as the end of measurement distance per Kelvin, that is, 26 mm for the current output LTS and 550 mm for the voltage output LTS. The LTS provides noncontact distance measurement by using angular relationships to calculate the distance between the object surface and the sensor. Figure 4 shows the measurement principle.

The laser beam travels from a light source to the object's surface along the illumination axis and is observed through a light spot. A position-sensitive detector photodiode array (PDA) based on the principle of a CCD determines the position of the light spot on the image plane.[23] The distance between the object surface and the aperture is determined by the included angle θ between the illumination and observation axes.[24] As the distance Δz increases, the angle θ decreases, leading to a lateral displacement $\Delta x'$ of the spot image on the image plane, described by

$$\Delta x' = \Delta z \cdot \sin(\theta). \tag{6}$$

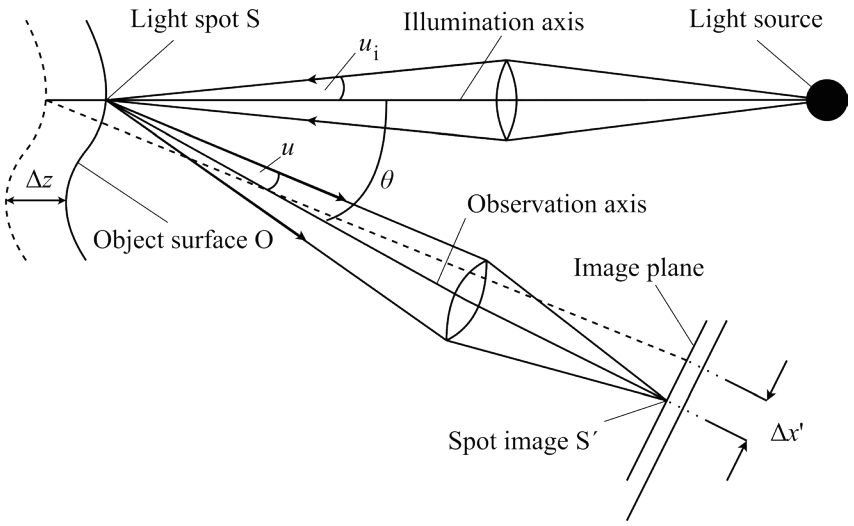

Fig. 4. Measurement principle for LTS.

A microcontroller converts this displacement into an output (electrical current or voltage) proportional to the distance, ensuring high linearity and measurement accuracy despite inherent measurement uncertainties.[25]

Since measurement systems consist of at least three components (sensor, cable, and measurement module), all components must be considered for the quantification of measurement uncertainty. Table 2 shows the characteristics of the measurement module used.

The Q.bloxx XL A107 measurement module from Gantner Instruments is designed for LTSs with current or voltage output signals and uses 24-bit delta-sigma modulation for analog-to-digital conversion. The repeatabilities of the module are ±1 μA for current output and ±200 μV for voltage output. Its temperature dependences are 0.1 μA/K for current output and 5 μV/K for voltage output. Owing to the significantly small temperature dependence of the module compared with the sensors, it can be neglected in the following analyses. The module records measurements at a sampling rate of 1 Hz.

Figure 5 shows the complete measurement chain. The LTS connects to the measurement module via a 4-pin cable.

- Sensor (LTS): LTSs have either a current or voltage output. In this work, either a 4–20 mA current output or a 0–10 V voltage output is provided.
- Cable: This consists of four twisted and shielded wires to minimize electromagnetic interference. Shorter cables are preferred to reduce resistance and thus measurement uncertainty.
- Measurement module: This contains analog and digital elements, including a program gain amplifier (PGA), an anti-aliasing filter, and an analog-to-digital converter (ADC), which converts analog signals to digital values. A field-programmable gate array (FPGA) performs digital processing, including filtering, calibration, and synchronization with the ADC.

Qualitative statements about the effect of different parameters on the measurement uncertainty of LTSs are discussed in company-related documents.[26] However, the quantitative

Table 2
Characteristics of the measurement module used.

Manufacturer	Gantner Instruments GmbH, Austria
Model name	Q.bloxx XL A107
ADC conversion	24 bits
Repeatability for current output (random measurement error)	±1 µA
Repeatability for voltage output (random measurement error)	±200 µV
Measurement rate in conducted experiments	1 Hz
Temperature dependence for current output	0.1 µA/K
Temperature dependence for voltage output	5 µV/K

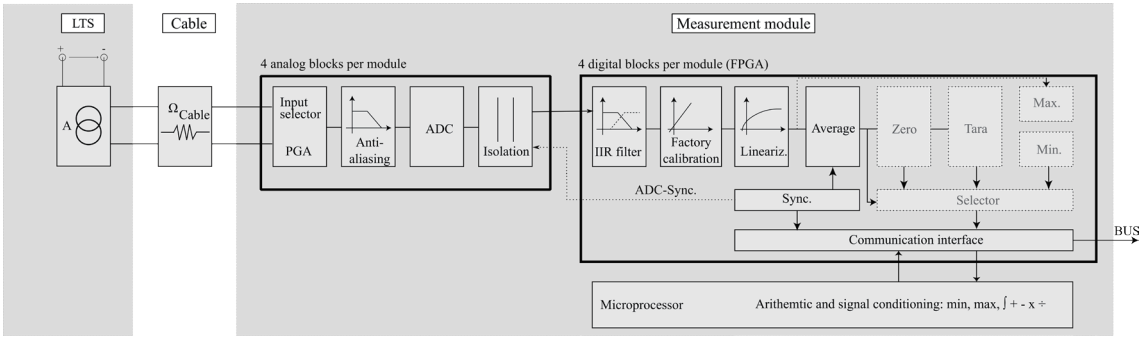

Fig. 5. Block diagram of the LTS measurement chain.

effect of the different components of the measurement chain on the overall measurement uncertainty is lacking and is therefore analyzed in Sect. 3.1.

2.3 Setup for time-invariant tests

To quantify the measurement uncertainty due to random effects in time-invariant measurement systems, the following parameters are varied:

- cable length for LTSs with current and voltage output signals,
- distance of the sensor to the measurement object, and
- type of measurement object surface.

The temperature is varied to quantify the measurement uncertainty due to systematic effects in time-invariant measurement systems. The climatic chamber adjusts temperatures between −10 and +50 °C (see Fig. 6).

This temperature curve covers the typical temperature range encountered in civil engineering structures. The nine simulated temperature levels are constant for 4 h each, followed by a 30-min adjustment to the next temperature level.

2.4 Setup for time-variant tests

The aging process of the measurement system is triggered by accelerated variations in temperature and humidity within the climatic chamber (time variance). It is assumed that the effects of scatter, temperature, and measurement system aging are independent of each other.

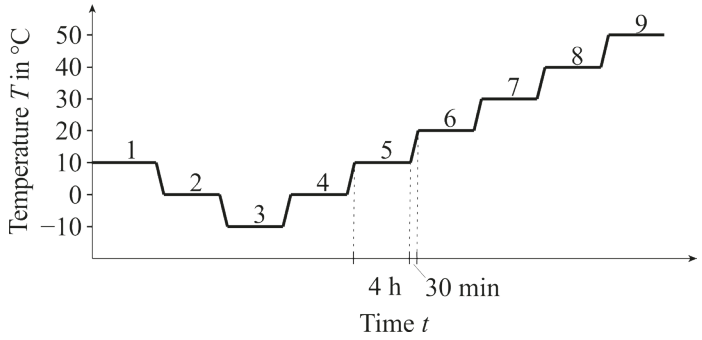

Fig. 6. Temperature curve for quantifying the temperature dependence of the measurement system (qualitatively).

This assumption holds as long as the measurement distance and the instrumentation hardware remain unchanged throughout the entire study, as ensured by the experimental setup shown in Fig. 3. Figure 7 illustrates the qualitative temperature and humidity curves during the time-variant tests.

The climate cycle comprises several phases, representing an accelerated day-night cycle by a factor of six. Four phases are defined according to the IEC 60068-2-2:2007 standard and Herrmann *et al.*'s research.[27,28]

Phase 1 (60 h) starts at T = 20 °C, held constant for 4 h. The temperature is then raised to T = 50 °C at 1.00 K/min, maintained for 4 h, and then lowered back to T = 20 °C. Relative humidity (RH) is maintained at 50%. This phase detects changes in temperature-dependent response. Phase 2 (60 h) is similar to Phase 1, but the temperature drops to T = −10 °C. Humidity control is limited, resulting in condensation and ice formation. In Phase 3 (60 h), the temperature is maintained at T = 20 °C and RH = 30%. This phase visualizes processes such as diffusion, moisture release, corrosion, and creep. Phase 4 (60 h) follows the temperature profile of Phase 1, but with RH = 80%. This phase detects changes in temperature behavior under high humidity. These phases are continuously repeated over the test period, starting with Phase 1 every 10 days.

3. Time-invariant and Time-variant Measurement System Behaviors

During the analysis, nine LTSs were tested: six with current output signals and three with voltage output signals. Since only current output LTSs are used in the aging tests (see Sect. 4), the number of voltage output LTSs is limited to three. Sections 3.1 and 3.2 are divided into effects on random and systematic errors.

Systematic errors, on the one hand, are primarily caused by the experimental setup or changing environmental conditions. These errors are not random and have the same effect when measurements are repeated under identical conditions. Consequently, systematic errors are not detectable under repeated conditions, although some can be corrected. A distinction is made between detectable and undetectable systematic errors. While undetectable systematic errors cannot be compensated for, detectable errors must be corrected, such as by temperature compensation (data normalization).

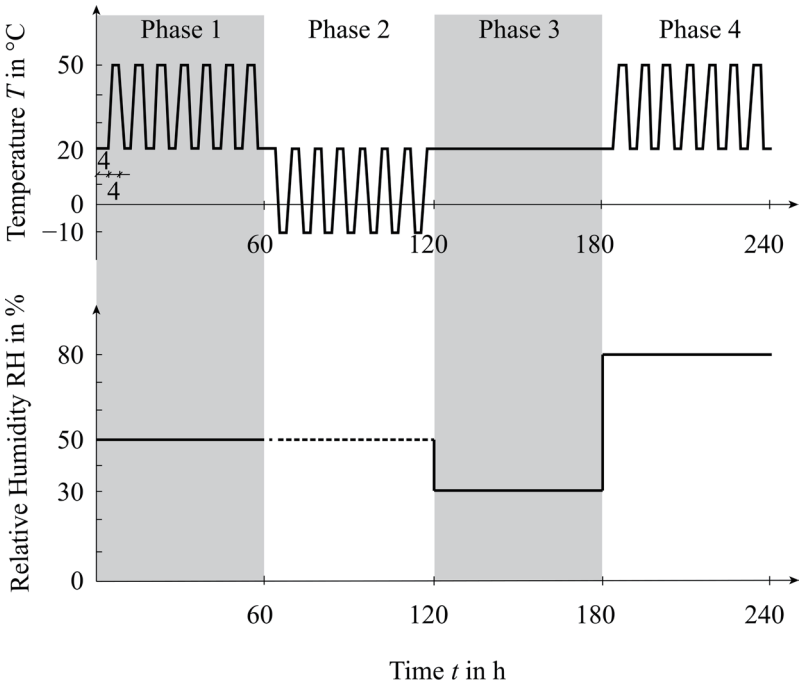

Fig. 7. Curve of temperature T and relative humidity *RH* as a function of time t to quantify the time dependence of the measurement system (qualitatively).

Random errors, on the other hand, arise from random sources in time and space, such as measurement noise. These errors are detectable under repeated conditions but cannot be corrected. Random errors can be partially estimated, but never fully described physically, as they are typically statistical in nature. In the case of multiple measurements, the values are scattered around a mean and follow a certain statistical distribution. To give readers an idea of the raw measurement data recorded, the data have been made publicly available in the Zenodo data repository.[29]

3.1 Measurement system component effects on random measurement error

To describe the effects of the system components on the random measurement error, the cable length, the distance between the sensor and the target, and the surface quality of the target are analyzed. During the tests, constant environmental conditions were maintained at $T = 20$ °C and $RH = 50\%$. The dispersion index was calculated as the twofold standard deviation (*SD*) of the output signals. In metrology, the twofold *SD* is commonly used as the measurement uncertainty because it provides a confidence level of at least 95% for the range of measured values, assuming a normal distribution. Three independent experiments were performed for each configuration, each with a measurement duration of 10 min. In total, 141 experiments were performed to characterize the random measurement uncertainty.

For in situ measurements, such as on engineering structures, longer cables from a few meters up to 100 m may be required,[30] so the effect of cable length on measurement error is of interest.

Cable lengths of 1, 5, 10, and 20 m are used in these tests, and the results for each configuration are shown in Fig. 8.

Figure 8(a) illustrates the effect of cable length on measurement uncertainty for current output sensors (LTS 2, LTS 4, and LTS 6). While LTS 2 shows an increase in uncertainty with longer cables, this trend is not consistent across all sensors. For LTS 4 and LTS 6, the uncertainty remains relatively stable, suggesting that cable quality, rather than length, is the dominant factor. This is particularly true for the current output LTSs, where the low impedance circuitry reduces sensitivity to cable capacitance and electromagnetic interference.

In contrast, Fig. 8(b) shows a different pattern for voltage output LTSs (LTS 7, LTS 8, and LTS 9), where the measurement uncertainty increases significantly with cable length. This is due to the higher susceptibility of voltage output circuits to cable capacitance and electromagnetic interference, resulting in greater signal distortion.

Figure 8(c) shows that for current output LTSs, the measurement uncertainty increases with the distance from the sensor to the target. The effect is more pronounced in Fig. 8(d) for voltage output LTSs, where the errors are particularly large at a distance of 300 mm, highlighting the significant effect of the measurement distance on the magnitude of the error.

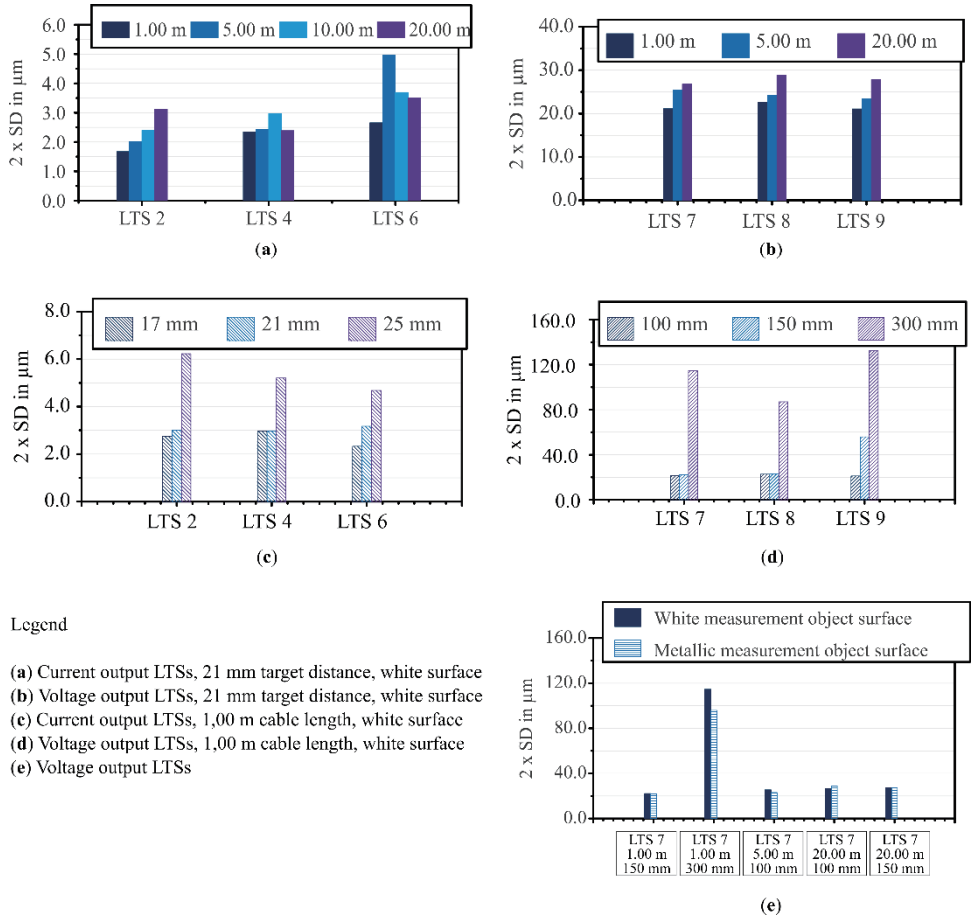

Fig. 8. (Color online) Results on measurement error effects with 1 Hz sampling frequency, T = 20 °C, and RH = 50%. (a) Cable lengths: 1, 5, 10, and 20 m; (b) cable lengths: 1, 10, and 20 m; (c) target distances: 17, 21, and 25 mm; (d) target distances: 100, 150, and 300 mm; (e) object surface type: white and metallic.

Figure 8(e) shows the effect of surface type on voltage output LTSs at various distances and cable lengths. At a distance of 300 mm, the measurement error varies considerably between surfaces, with darker, metallic surfaces producing lower errors than lighter, reflective surfaces. However, at shorter distances (100 or 150 mm), surface type has a minimal effect.

To minimize random measurement errors, it is recommended to use LTSs with current output signals and short, low-capacitance cables, and to place the sensor as close to the target as possible. In addition, selecting an LTS with a narrow measurement range and using twisted and shielded cables can further reduce electromagnetic interference.

3.2 Temperature effect on systematic measurement error

On the basis of the results described in Sect. 3.1, the optimal measurement configuration was selected: an LTS sensor with current output, minimized cable length, and minimized target distance. This configuration was subjected to varying temperatures to evaluate systematic measurement errors. Figure 9 shows the output signal response of LTS 4 under different temperature conditions, using 20 °C as a reference with an offset change baseline of $\Delta d = 0$ µm.

In the temperature range from −10 to +50 °C, Fig. 9(a) shows an offset change between −35 and +5 µm. The largest offset occurred at +50 °C, while at −10 °C, the output signal showed the largest scatter. Overall, the measurement signal decreased with increasing temperature relative to 20 °C and also decreased as the temperature dropped below 20 °C, reaching a minimum at −10 °C.

These observations underscore the importance of understanding the temperature-dependent behavior of the sensors themselves for monitoring engineering structures. Accurately distinguishing between actual structural damage and systematic effects on the measurement system requires careful consideration of these temperature effects.[31]

Using the raw data from Fig. 9(a), we calculated the arithmetic means and the twofold standard deviations for each temperature level, as shown in Fig. 9(b). This analysis led to the determination of a temperature-dependent transfer function from −10 to +50 °C, which describes the behavior of the measurement system under varying temperature conditions. Polynomial regression was applied to the arithmetic mean and their corresponding standard deviations, and

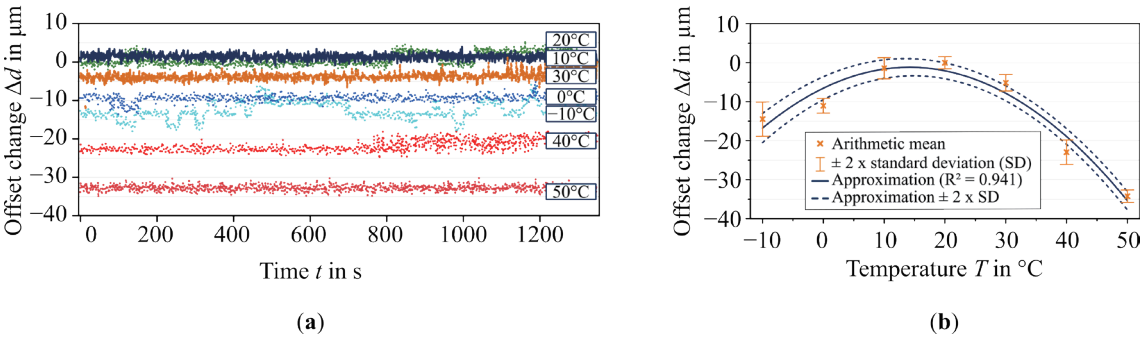

Fig. 9. (Color online) Current output LTS 4 signal with RH = 50%, cable length of 1 m, and a distance to the measurement object of 21 mm. (a) Raw data signal and (b) temperature-dependent transfer function.

the Akaike Information Criterion (AIC) was used to select the best-fitting model. This criterion, widely used in statistics, balances model accuracy with complexity.[32] The analysis then identified a second-degree polynomial as the most appropriate function to mitigate systematic temperature effects. The results indicate that the LTS sensor has the least measurement variation at 20 °C, while the greatest uncertainty occurs at −10 °C. Given that the climatic chamber used in the experiment is an isolated environment with minimal external influences, and that the LTS experimental setup rests on vibration-damping elastomeric bearings, the measurement uncertainty can be attributed to the measurement system components. To minimize this uncertainty in practice, extreme temperatures should be avoided, but this is often impractical in SHM applications. Therefore, temperature-dependent variations in measurement uncertainty must be considered in the modeling of measurement system behavior.

These test results establish a reference baseline for the behavior of the measurement system. Time-varying results are compared with this baseline.

3.3 Measurement drift and measurement error over time

The measurement system configuration described in Sect. 3.2 (LTS with current output, minimized cable length, and minimized target distance) was subjected to an aging process in the climatic chamber as described in Sect. 2.4. The system was exposed to varying temperatures and relative humidities over 240 h intervals. After each aging period of 240 h, a comparative test was performed under the conditions described in Sect. 2.3, specifically with a temperature variation at a relative humidity of 50%, to identify potential changes in baseline condition and therefore aging effects in the measurement system. Figure 10 illustrates the effects due to time-variant system behavior.

Figure 10 shows the temperature-dependent transfer function over time as a 3D and a 2D plot, respectively, describing in the 3D plot the mean values of the transfer function for different temperatures over the aging period at discrete time points, interpolating between the aging intervals. The 2D plot offers a detailed perspective on the offset change over time at a constant temperature of 20 °C and a relative humidity of 50%, including the twofold standard deviation at specific time points. It is notable that the transfer function changes over time, not in a systematic manner but in a random manner (there is no constant factor that changes the transfer function in total). In the reference state at time $t = 0$ h, the transfer function is analogous to that depicted in Fig. 9(b). The global maximum of the transfer function occurs at 20 °C and $t = 0$ h. Throughout the study period, the local maximum of each transfer function remains at 20 °C. However, a closer look reveals significant differences. After $t = 960$ h, a global minimum of the offset change Δd is observed at 50 °C. At 1440 h, the transfer function has deviated significantly from the reference state.

Specifically, the 2D plot in Fig. 10 shows that both the mean and the twofold standard deviation of the measurement signal fluctuate significantly over time. These discrete comparison measurements at $T = 20$ °C and $RH = 50\%$ were conducted at $t = 0$, 720, 960, 1200, and 1440 h. It was assumed that significant aging effects would primarily occur at later stages, meaning that the measurement system was expected to remain stable for a prolonged period before notable

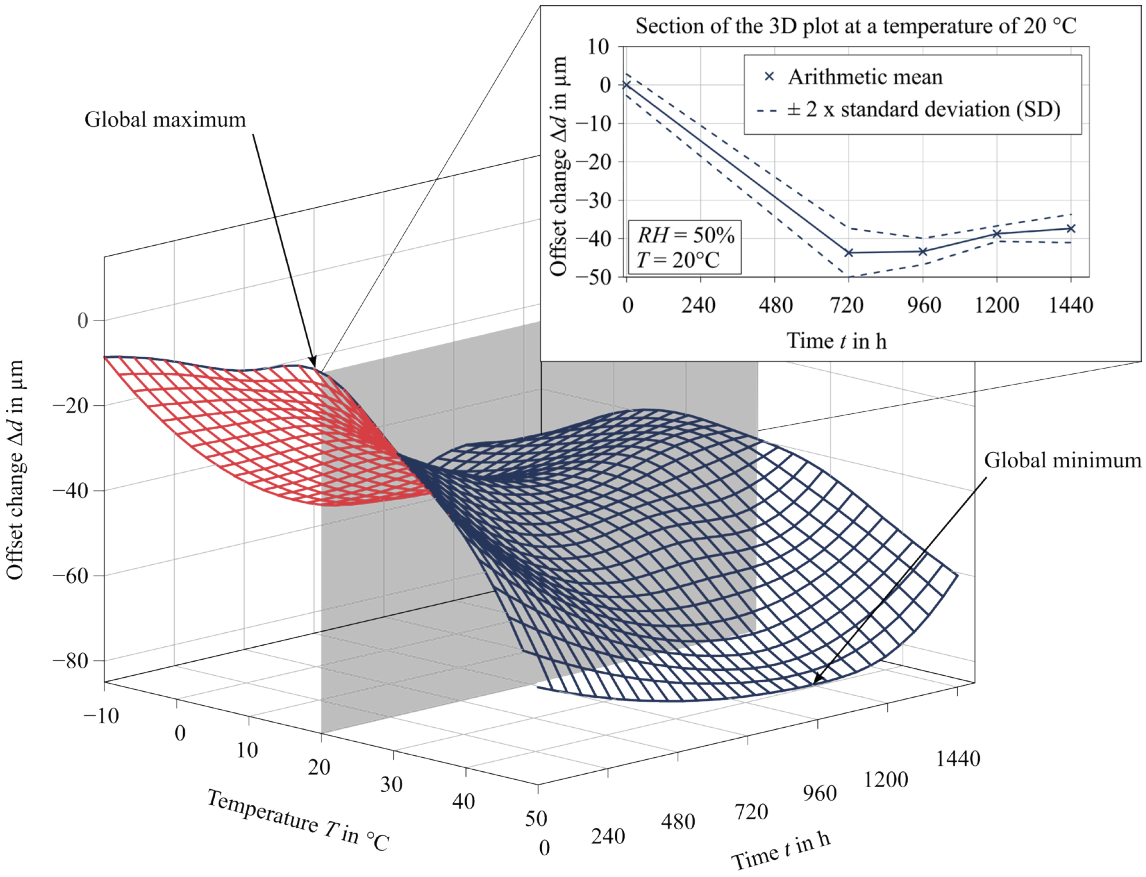

Fig. 10. (Color online) 3D plot illustrating the temperature-dependent transfer function over time at a constant relative humidity of 50%. Additionally, a detailed view of the offset change over time at a fixed temperature of 20 °C and a relative humidity of 50% is provided, including the twofold standard deviation at discrete time points.

offset changes appeared. However, the results indicate that the most significant variations occurred during the early phase, suggesting that future studies should include more frequent comparison measurements within the first 720 h to better capture these initial fluctuations. After 720 h, the measurement system stabilizes and less significant changes are observed compared with the initial period. Practically, this suggests that the measurement system should be allowed a "settling period" at the measurement site before data collection is started.

The magnitude of the time-variant offset change Δd in the LTS measurement system, illustrated in the 2D plot of Fig. 10, shows a mean offset change of approximately 45 µm between 0 and 720 h. Between 720 and 1440 h, this offset change decreases to about 7 µm. To put these values into the perspective of civil engineering structure monitoring, the required measurement accuracy for crack monitoring on concrete surfaces of prestressed concrete bridges (e.g., the Carola Bridge in Dresden, Germany, which collapsed in 2024) is 20–50 µm.[33,34] The LTS measurement system can meet these accuracy requirements when it is in a healthy state. However, if the measurement system is subject to aging and does not have a settling period, time-variant changes of a similar magnitude can lead to the misinterpretation of the measured

values. This in turn could lead to the unnecessary bridge downtime and loss of confidence in the monitoring system.

Given these potential issues, the question arises as to how to address the time-variant behavior of the measurement system. Time-dependent fluctuations affect both the temperature-related systematic error and the random measurement error at each temperature. Consequently, Eq. (3) must be adopted to explicitly incorporate time dependence in all parameters $\bar{y}(t)$, $\epsilon_{Temperature}(t)$, and $2 \cdot \sigma(t)$:

$$y(t) = \bar{y}(t) + \epsilon_{Temperature}(t) \pm 2 \cdot \sigma(t). \tag{7}$$

For the specific implementation of time variance within the investigated use case, the results regarding random and systematic measurement errors are used to incorporate time variance.

The temperature-dependent transfer function is optimally approximated by a second-degree polynomial, and random measurement errors are accounted for by the twofold standard deviation. Thus, the behavior of the measurement system is described by the mathematical model:

$$y(\theta_i(t), T) = a_0 \cdot \theta_1(t) \cdot T^2 + a_1 \cdot \theta_2(t) \cdot T + a_2 \cdot \theta_3(t) \pm 2 \cdot \sigma \cdot \theta_4(t), \tag{8}$$

where T is temperature, t is time, and $\theta_i(t)$ represents a parameter for the time-dependent adjustment of the analytical model. Equation (8) forms the basis for handling time-variant measurement systems with BMU.

4. Handling Time Variance with BMU

Since a significant difference in the behavior of the measurement system has been found between 0 and 720 h (see Fig. 10), the change in the mathematical model over this period must be taken into account and compensated for by BMU. Instead of a complex manual procedure to update the model, MCMC and TMCMC samplers are used. The objective is to compare the results of these two samplers with the results of the manual solution and to recommend the appropriate BMU sampler for aging monitoring systems.

4.1 Implementation of MCMC and TMCMC samplers within BMU

The following pseudocode in Table 3 describes the steps to perform modeling and parameter fitting using the MCMC and TMCMC samplers for observational data as a function of temperature.

Algorithm 1 outlines the MCMC sampling process, beginning with the initialization of the model parameters, including the coefficients of a second-degree polynomial (a_0, a_1, a_2) and the temperature-dependent noise term (σ). This algorithm generates a Markov chain by perturbing the current parameter values to suggest new ones. The log-likelihood of the new parameters is

Table 3
Pseudocode for BMU with MCMC and TMCMC sampling.

```
Input Temperature and distance measurements for the state of an aged measurement system
Parameter initialization
    Define the a priori parameters for the polynomial (a_0, a_1, a_2)
    Define the initial values for the temperature-dependent noise term (sigma_dict_prior)
Model function
    Define a model function (here: second-degree polynomial function)
        def model (temp, a_0, a_1, a_2):
            return a_0 + a_1 * temp + a_2 * temp**2
Log-likelihood function
    Calculate the log-likelihood, which considers the difference between prediction and observations:
    def log_likelihood (a_0, a_1, a_2, observations, temperatures):
        model_predictions = np.array([model(t, a_0, a_1, a_2) for t in temperatures])
        residuals = observations - model_predictions
        log_likelihood_value = np.sum(norm.logpdf(residuals, loc=0, scale=1))
        return log_likelihood_value
```

1.6:	**Algorithm 1** MCMC sampling	2.6:	**Algorithm 2** TMCMC sampling
1.7:	*Initialize MCMC parameters and settings (initial values, step size)*	2.7:	*Set number of stages (num_stages)*
1.8:	***for** n_iterations in 1 to n_iterations:*	2.8:	*Start with β=0 (uniform distribution), and gradually transition to β=1 (target distribution) as the stages progress*
1.9:	*Generate new parameter values (a_0, a_1, a_2) by interfering with the current values*	2.9:	*Initialize TMCMC parameters and settings (initial values, step size)*
1.10:	*Update the temperature-dependent noise term (sigma_dict)*	2.10:	***for** each stage from 1 to num_stages:*
1.11:	*Calculate the log-likelihood for the new parameters*	2.11:	*Calculate β for the current stage:*
1.12:	***If** log-likelihood for new parameters is better than current log-likelihood:*	2.12:	*β = stage / num_stages*
1.13:	*Accept new parameters*	2.13:	*Calculate the log-likelihood for the new parameters and noise term, weighted by β.*
	(a_0, a_1, a_2) and noise term	2.14:	***If** new log-likelihood is better (or passes the Metropolis criterion)*
1.14:	***Otherwise:***	2.15:	*accept the new parameters and*
1.15:	*Keep current parameters and noise term*		*noise term*
		2.16:	***Otherwise***
1.16:	*Save the parameter chains*		*keep the current parameters*
1.17:	***end***	2.17:	***end***

```
Model predictions and uncertainty
    Calculate means and standard deviations of model predictions based on the MC chain
```

calculated, and new values are accepted if they improve on the current ones. This iterative process continues for a fixed number of iterations, and the parameter chains are stored for later analysis.

Algorithm 2 describes TMCMC, a modified version of MCMC in which the temperature of the target distribution is adjusted in several steps. Initially, β is set to 0 and gradually increased to 1. At each step, the log-likelihood is calculated with the current β, accepting new parameters if they improve the log-likelihood or satisfy the Metropolis criterion.

The main differences between MCMC and TMCMC lie in their parameter transition strategies. MCMC uses a fixed step size, whereas TMCMC uses a stepwise transition, which

improves the exploration of parameter space. The dynamic temperature variable of TMCMC allows for a more flexible fit, which helps to avoid local maxima. Specifically, this advantage of TMCMC sampling means that the algorithm is not limited to a second-degree polynomial, but can update between arbitrarily complex, predefined mathematical models. Although MCMC is generally less computationally intensive, TMCMC may be more advantageous for complex models such as those describing measurement system behavior.

The initial mathematical model according to Eq. (8) is available at the time t = 0 h and is given by

$$y\left(\theta_i\left(t=0h\right),T\right)=2.029\cdot T^2+0.635\cdot T-0.036\pm 1.293\,\mu m\,. \tag{9}$$

The process of updating the measurement system behavior over time is automated using the MCMC and TMCMC samplers. The results of BMU using the two samplers are shown in the next subsection.

4.2 Results and discussion

In addition to the final model updates in Fig. 11, the trace plots and pair plots are compared to analyze the results of the two samplers in BMU. In Fig. 11, the orange dots represent the measured distances as a function of temperature. The blue line represents the mean of the updated mathematical model, whereas the transparent blue lines represent the bounds of the twofold standard deviation, defined as temperature-dependent noise at temperatures in 10 K steps, starting from −10 °C and interpolating linearly between the temperatures.

The MCMC-generated model in Fig. 11(a) shows good fit in the temperature range from 10 to 50 °C, while the model accuracy decreases slightly at lower temperatures (–10 to 0 °C). In contrast, the TMCMC-generated model in Fig. 11(b) gives a worse result than the MCMC one.

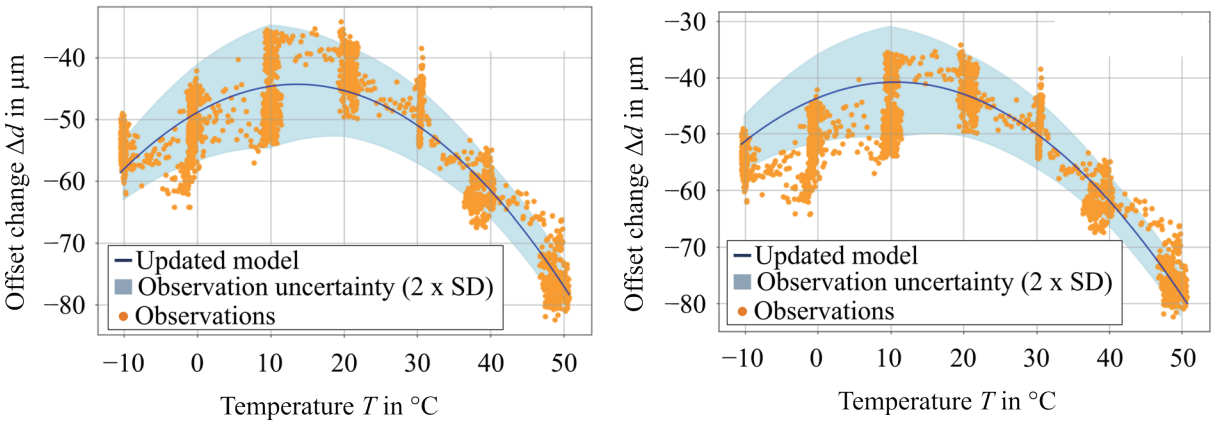

Fig. 11. (Color online) Results of BMU using (a) MCMC and (b) TMCMC samplers. The orange dots represent the distances measured by the LTS. The blue line represents the mean of the updated model, and the transparent blue lines indicate the twofold standard deviation of the observations fitting the updated model.

Particularly at low temperatures from −10 to 10 °C, the approximation of the MCMC sampler is better.

One reason for the slightly better estimation is the burn-in phase in the MCMC sampler. This phase allows the MCMC sampler to move away from an unfavorable starting point and achieve a more stable posterior distribution. The use of a burn-in phase (discarding the first 15% of iterations, a common practice in science) improves the stability of the MCMC sampler, whereas the TMCMC sampler uses progressive weighting and incorporates multiple mathematical models into the updating process. This makes the TMCMC sampler more flexible concerning complex aging processes of the measurement system.

Looking at the trace plots of the parameters a_0, a_1, and a_2 as a function of the number of sampling iterations, the differences between the MCMC and TMCMC samplers become clear.

A total of one million iterations were performed as part of BMU. In the MCMC sampler, 15% of iterations, or 150000 values, were defined as the burn-in phase. This can also be seen in the trace plots: Fig. 12(a) shows 850000 iterations, whereas Fig. 12(b) considers all 1000000 iterations. The MCMC sampler converges after about 450000 iterations, whereas the TMCMC sampler requires about 600000 iterations. Ultimately, both samplers identify a second-degree polynomial as the best-fitting model.

Figure 13 shows the pair plots for MCMC and TMCMC. Figure 13(a) again shows the model generated by MCMC sampling, and Fig. 13(b), the model generated by TMCMC sampling.

The diagonal elements of the figure show the posterior histograms for the three updated parameters. The off-diagonal elements show the scatter plots between two of these parameters. The TMCMC sampler shows more data points because it allows a continuous improvement of the iteration results compared with the MCMC sampler. A strong correlation can be seen between the parameters a_1 and a_0. In addition, the mean value in the final updated process is represented by a red vertical dashed line.

The calculated mean values of the second-degree polynomial and the approximated uncertainty of the measurement system are compared with a manual calculation result in Table 4. The parameters a_0, a_1, and a_2 were manually calculated by the least squares method. The

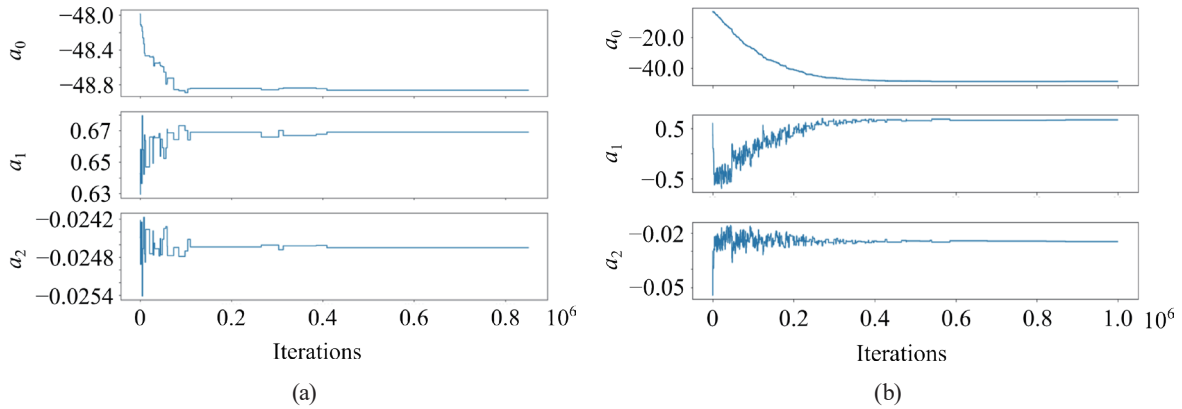

Fig. 12. (Color online) Trace plots of parameters a_0, a_1, und a_2. (a) MCMC and (b) TMCMC samplers.

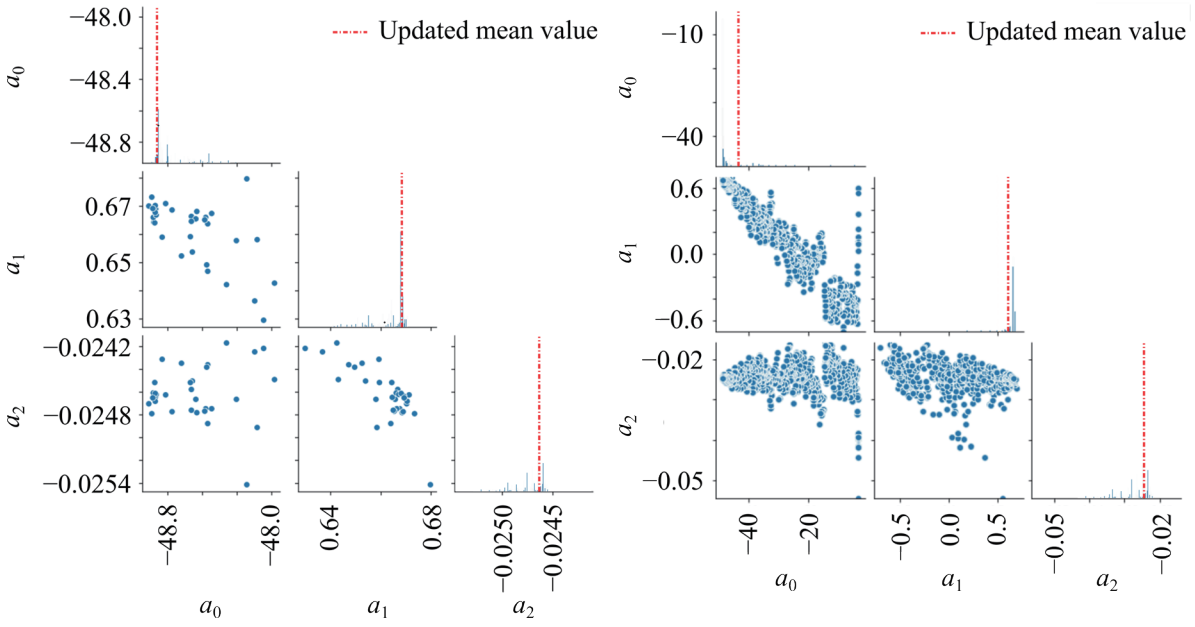

Fig. 13. (Color online) Pair plots of posterior distributions. (a) MCMC and (b) TMCMC samplers.

Table 4
Comparison of accuracies of MCMC and TMCMC samplers versus manual solution (bias in %).

	α_0	α_1	α_2	$2 \cdot \sigma$
Manual	−48.81	0.67	−0.025	6.48 µm/m
MCMC	−48.85 (−0.08%)	0.67 (±0.00%)	−0.025 (±0.00%)	6.50 µm/m (+0.30%)
TMCMC	−45.00 (+7.91%)	0.52 (−22.39%)	−0.024 (+0.04%)	6.40 µm/m (−1.23%)

twofold standard deviation was determined from the temperature-dependent noise as the mean of the noise component per temperature level. The values listed in the first row of Table 4 serve as a reference and are used for the quantified comparison with the results of the MCMC and TMCMC samplers.

The BMU models agree well in their accuracy, with the MCMC sampler performing slightly better than the TMCMC sampler. However, both methods accurately capture the uncertainty of the system and provide stable approximations. While the MCMC sampler provides more accurate results, the TMCMC sampler is particularly valuable owing to its flexibility in considering different mathematical models. This allows an analytical description of the best possible model, which is critical for long-term reliability analysis, especially when quantifying uncertainties in critical temperature ranges.

The use of BMU makes it possible to use the a priori knowledge of the measurement system behavior to continuously adjust the model without having to remove or recalibrate the sensor. Instead, calibration is performed during operation, allowing, for example, drift due to aging to be compensated in real time. In this way, BMU provides a flexible solution for time-variable calibration, the quantification of uncertainty, and the integration of prior knowledge in a measurement system.

5. Conclusion and Outlook

In this paper, we presented a novel approach to account for aging effects in monitoring systems, which are often incorrectly assumed to be time-invariant. With LTSs as a case study, random, systematic, and time-dependent measurement errors were experimentally investigated and mathematically modeled in more than 140 subtests. In addition, a method to compensate for the time-dependent behavior was validated. BMU proved to be particularly suitable for the compensation of aging monitoring systems, as it integrates the mathematical model, takes into account measurement uncertainties, and remains interpretable at the same time.

The main findings are as follows:

- Random and systematic measurement errors: LTSs with current output signals were insensitive to cable length, whereas LTSs with voltage outputs showed significant errors due to cable length and distance to the target. To minimize random errors, LTSs with current output, short cables with low capacitance, and the close positioning of the sensor to the measurement object are recommended. Temperature systematically affected the measurement system, requiring compensation by a temperature-dependent transfer function optimized by the AIC.
- Aging and time-dependent behavior: Experiments in the climatic chamber showed that temperature effects led to measurement drift and temporal variation, indicating age-related drift. This temperature-dependent behavior was described by a second-degree polynomial model over time, which showed significant differences, especially at the beginning of the aging process.
- Compensation of time-dependent behavior: BMU enables real-time calibration and uncertainty quantification in dynamic measurement systems, improving reliability without sensor removal or laboratory recalibration. The BMU models demonstrate high accuracy, with the MCMC sampler slightly outperforming the TMCMC sampler. While the MCMC sampler yields more precise results, the TMCMC sampler stands out for its flexibility in handling different mathematical models.

In this paper, we underscored the importance of considering the time-dependent behavior of measurement systems, as the measurement drift can be of the same order of magnitude as the displacement of the measurement object due to object condition changes. The BMU application is therefore critical for long-term monitoring, as undetected sensor degradation could lead to costly or dangerous misjudgments in structural monitoring. This approach to compensate for aging effects significantly increases the accuracy of the measurement system over time and contributes to improving the longevity and reliability of monitoring systems.

Data availability

All raw data, including test program documentation, are uploaded to the Zenodo data repository. The data can be accessed via the following link: https://zenodo.org/records/7178305

Acknowledgments

This research is funded by the German Research Foundation (Deutsche Forschungsgemeinschaft, DFG), as part of the Collaborative Research Centre 1463 (Sonderforschungsbereich, SFB 1463) "Integrated Design and Operation Methodology for Offshore Megastructures" (subproject C01, project number 434502799). This article represents the opinions of the authors and does not mean to represent the position or opinions of the funding entities.

References

1 P. Rizzo and A. Enshaeian: Sensors **21** (2021) 4336. https://doi.org/10.3390/s21134336
2 T. Hsieh, Y. Chou, H. Lai, and Y. Chien: Sens. Mater. **36** (2024) 2813. https://doi.org/10.18494/SAM4882
3 L. Wu, K. Wang, H. Gao, L. Qiang, and D. Yang: Sens. Mater. **36** (2024) 2765. https://doi.org/10.18494/SAM4878
4 L. Jiang, D. Djurdjanovic, J. Ni, and J. Lee: Engineering Asset Management, J. Mathew, J. Kennedy, L. Ma, A. Tan, and D. Anderson, Eds. (Springer, London, 2006) pp. 1252–1260. https://doi.org/10.1007/978-1-84628-814-2_138
5 G. Konstantinidis: Proc. 2005 Quantitative Nondestructive Evaluation (AIP, 2006) 1702–1709. https://doi.org/10.1063/1.2184726
6 J.-H. Bartels, R. Xu, C. Kang, R. Herrmann, and S. Marx: Metrology **4** (2024) 46. https://doi.org/10.3390/metrology4010004
7 C. Farrar and K. Worden: Phil. Trans. R. Soc. A. **365** (2007) 303. https://doi.org/10.1098/rsta.2006.1928
8 A. Turnbull and J. Carroll: Energies **14** (2021) 1. https://doi.org/10.3390/en14164922
9 E. Cross, K. Koo, J. Brownjohn, and K. Worden: Mech. Syst. Signal Process. **35** (2013) 16. https://doi.org/10.1016/j.ymssp.2012.08.026
10 R. Patton: Proc. IEE Colloquium on Condition Monitoring and Fault Tolerance (1991) 127.
11 K. Smarsly and K. Law: Adv. Eng. Software **73** (2014) 1. https://doi.org/10.1016/j.advengsoft.2014.02.005
12 D. Jana, J. Patil, S. Herkal, S. Nagarajaiah, and L. Duenas-Osorio: Mech. Syst. Signal Process. **169** (2022) 108723. https://doi.org/10.1016/j.ymssp.2021.108723
13 J. Kullaa: Mech. Syst. Signal Process. **25** (2011) 2976. https://doi.org/10.1016/j.ymssp.2011.05.017
14 T. Al-Zuriqat, C. Chillón Geck, K. Dragos, and K. Smarsly: Infrastructures **8** (2023) 39. https://doi.org/10.3390/infrastructures8030039
15 J.-H. Bartels, T. Potthast, S. Möller, T. Grießmann, R. Rolfes, M. Beer, and S. Marx: Proc. 11th European Workshop on Structural Health Monitoring (EWSHM, 2024) 1–10. https://doi.org/10.58286/29699
16 A. Lye, A. Cicirello, and E. Patelli: Mech. Syst. Signal Process. **159** (2021) 107760. https://doi.org/10.1016/j.ymssp.2021.107760
17 J. Beck and L. Katafygiotis: J. Eng. Mech. **124** (1998) 455. https://doi.org/10.1061/(ASCE)0733-9399(1998)124:4(455)
18 T. G. Ritto, R. Sampaio, and R. R. Aguiar: Mech. Syst. Signal Process. **68** (2016) 176. https://doi.org/10.1016/j.ymssp.2015.08.010
19 R. Rastogi, S. Ghosh, A. Ghosh, K. Vaze, and P. Singh: Fatigue Fract. Eng. Mater. Struct. **40** (2017) 145. https://doi.org/10.1111/ffe.12486
20 R. Rocchetta, M. Broggi, Q. Huchet, and E. Patelli: Mech. Syst. Signal Process. **103** (2018) 174. https://doi.org/10.1016/j.ymssp.2017.10.015
21 E. Jaynes: Maximum-Entropy and Bayesian Methods in Science and Engineering, G. J. Erickson and C. R. Smith, Eds. (Springer, Dordrecht, 1988) 1st ed., pp. 25–29. https://doi.org/10.1007/978-94-009-3049-0_2
22 Baumer Electric AG: https://www.baumer.com/de/en/product-overview/distance-measurement/laser-distance-sensors/performance-laser-distance-sensors/miniature-sensors-up-to-120-mm/om20-p0026-hh-yin/p/42835 (accessed January 2025).
23 R. Dorsch, G. Häusler, and J. Herrmann: Appl Opt. **33** (1994) 1306. https://doi.org/10.1364/AO.33.001306
24 M. Löffler-Mang: Optische Sensorik, M. Löffler-Mang, Eds. (Vieweg + Teubner Verlag, Wiesbaden, 2012) 1st ed., pp. 172–177. https://doi.org/10.1007/978-3-8348-8308-7

25 J.-H. Bartels, D. Gebauer, and S. Marx: Bautechnik **100** (2023) 67. https://doi.org/10.1002/bate.202200102
26 Baumer Electric AG: https://www.baumer.com/medias/__secure__/Baumer_OM20-30-IO-Link_DE_V6_MNL.pdf?mediaPK=9005775618078 (accessed January 2025).
27 DIN EN 60068-1:2015-09: Environmental testing - Part 1: General and guidance (IEC 60068-1:2013); German version EN 60068-1:2014: https://www.dinmedia.de/en/standard/din-en-60068-1/236175130 (accessed January 2025).
28 R. Herrmann, M. Stockmann, and S. Marx: Bautechnik **92** (2015) 451. https://doi.org/10.1002/bate.201500018
29 J.-H. Bartels: Zenodo 1.1 (2022). https://doi.org/10.5281/zenodo.11657891
30 Y. Luo, Y. Chen, H. Wan, F. Yu, and Y. Shen: J. Civ. Struct. Health Monit. **11** (2021) 381. https://doi.org/10.1007/s13349-020-00459-4
31 C. Farrar, H. Sohn, and K. Worden: https://www.osti.gov/biblio/975664 (accessed January 2025).
32 H. Akaike: IEEE Trans. Autom. Control **19** (1974) 716. https://doi.org/10.1109/TAC.1974.1100705
33 Eurocode 2: Design of concrete structures - Part 1-1: General rules and rules for buildings; German version EN 1992-1-1:2004 + AC:2010. https://dx.doi.org/10.31030/1723945
34 Institute of Concrete Structures TUD Dresden University of Technology: https://tu-dresden.de/bu/bauingenieurwesen/imb/das-institut/news/einsturz-der-carolabruecke-in-dresden?set_language=en (accessed January 2025).

About the Authors

Jan-Hauke Bartels was born in Germany in 1994. He received his M. Sc. degree in structural engineering from Leibniz University Hannover in 2020. Since then, he has been a research assistant at the Institute of Concrete Structures, TU Dresden, where he is pursuing his Ph.D. degree in civil engineering. His research focuses on the condition assessment of measurement systems and the application of the developed techniques to structural health monitoring systems in the field of civil engineering structures. (jan-hauke.bartels@tu-dresden.de)

Steffen Marx was born in Germany in 1969. He received his diploma in civil engineering from the University of Weimar in 1995 and his Ph.D. degree from Bauhaus University of Weimar in 1999. He was an honorary professor at TU Dresden (2007–2010) and a visiting professor at UC San Diego (2010–2011). From 2011 to 2020, he was a professor at Leibniz University Hannover. Since 2020, he has been holding the DB Netz AG Endowed Professorship at the Institute of Concrete Structures at TU Dresden. His research focuses on structural health monitoring for bridges and wind turbines, as well as the impact and fatigue of concrete structures.
(steffen.marx1@tu-dresden.de)